J. Fluid Mech. (2002), *vol.* 456, *pp.* 137–159. © 2002 Cambridge University Press
DOI: 10.1017/S0022112001007716 Printed in the United Kingdom

An experimental investigation of MHD quasi-two-dimensional turbulent shear flows

By KARIM MESSADEK AND RENE MOREAU

Laboratoire EPM Madylam, ENSHMG BP 95, 38402 Saint Martin d'Heres Cedex, France

(Received 17 October 2000 and in revised form 9 July 2001)

An extensive experimental study is carried out to examine the properties of a quasi-two-dimensional MHD turbulent shear flow. Axisymmetric shear of a mercury layer is enforced by the action of a steady vertical magnetic field and a radial horizontal electric current flowing between a ring set of electrodes and a cylindrical wall. This shear layer is unstable, and the properties of the turbulent flow are studied for a wide range of Hartmann (up to 1800) and Reynolds numbers (up to 10^6). The mean velocity profiles exhibit a turbulent free shear layer, of thickness larger than that predicted by the laminar theory by two orders of magnitude. The profiles yield the expected linear dependence between the total angular momentum and the electric current when the magnetic field is large enough, but demonstrate a systematic deviation when it is moderate ($Ha \lesssim 250$). The quasi-two-dimensional turbulence is characterized by an energy transfer towards the large scales, which leads to a relatively small number of large coherent structures. The properties of these structures result from the competition between the energy transfer and the Joule dissipation within the Hartmann layers. In the intermediate range of wavenumbers ($k_\ell < k < k_i$, where k_ℓ is the integral-length-scale wavenumber and k_i the injection wavenumber), the energy spectra exhibit a power law close to $k^{-5/3}$ when the Joule dissipation is weak and close to k^{-3} when it is significant. The properties of the turbulent flow in this latter regime depend on only one non-dimensional parameter, the ratio $(Ha/Re)(l_\perp/h)^2$ (Ha is the Hartmann number, Re the Reynolds number based on the cell radius, $l_\perp$ a typical transverse scale, and h the layer width).

1. Introduction

The tendency of MHD flows on the laboratory scale, where the magnetic Reynolds number is much smaller than unity ($R_m = \mu\sigma UL \ll 1$, where μ denotes the magnetic permeability, σ the electrical conductivity, U and L are a typical velocity and length scale respectively), to form quasi-two-dimensional structures is now well understood (e.g. Moreau 1990). MHD flows subject to a sufficiently strong uniform magnetic field (flows around bodies, Hunt & Ludford 1967, Mück *et al.* 2000; buoyancy-driven flows, Alboussière *et al.* 1997, Davoust *et al.* 1999) exhibit this behaviour, which may be understood as reminiscent of Alfvén wave propagation when R_m becomes very small. Sommeria & Moreau (1982) showed that this Alfvén wave propagation degenerates into a unidirectional diffusion in the magnetic field direction with a magnetic diffusivity of $D_m = (\sigma B^2/\rho)l_\perp^2$. The time scale characteristic of the establishment of two-dimensionality between Hartmann walls which are a distance h apart is $\tau_{2D} = (\rho/\sigma B^2)(h^2/l_\perp^2)$ (B stands for the magnetic field intensity and ρ for

fluid density). Note that the first qualitative experimental evidence of this behaviour was given by Lenhert (1955) more than 30 years ago.

In the particular case of turbulence, the tendency of an initially three-dimensional turbulent flow to become two-dimensional was first observed by Kolesnikov & Tsinober (1972). But the most specific experiment to investigate this phenomenon was performed by Alemany *et al.* (1979), who suggested a first theoretical interpretation and derived the main scaling laws, in particular the ratio between the parallel and perpendicular length scales, evolving with time (or with distance from the grid that generates the turbulence) as $l_{\parallel}/l_{\perp} = (\sigma B^2 t/\rho)^{1/2}$. They also numerically modelled the development of this anisotropy, based on an EDQNM formulation adapted to the MHD equations, which was in good agreement with their experimental results. Davidson (1997) stated that this evolution towards a quasi-two-dimensional regime is a consequence of the invariance of the angular momentum component parallel to the magnetic field, whereas the perpendicular components decay exponentially ($\simeq \exp(\sigma B^2 t/\rho)$).

Neither these experiments (e.g. Alemany *et al.* 1979), nor the theories (Alemany *et al.* 1979 and Davidson 1997) considered the Hartmann walls, which are likely to limit the elongation of the turbulent eddies in the magnetic field direction. Therefore, in these first investigations the induced electric current cannot be zero and the energy decay by the Joule effect remains important and finally leads to a full suppression of the turbulence. But, in the presence of insulating Hartmann walls, the two-dimensionality may be well established after the time τ_{2D} (Sommeria & Moreau 1982). The electric current within the core of the turbulent flow disappears and the only remaining dissipation takes place within the thin Hartmann layers present at both ends of the eddies. The thickness of this layer in which the velocity exponentially approaches zero is $(1/B)\sqrt{\rho\nu/\sigma}$ (ν denotes the viscosity which controls the dissipation at the same rate as the electric resistivity). The Hartmann-layer damping time scale $\tau_H = (h/B)\sqrt{\rho/\sigma\nu}$ (Sommeria & Moreau 1982) may be much longer than the Joule time scale of initially isotropic turbulence $\tau_J = \sigma/\rho B^2$. Therefore, a high level of quasi-steady two-dimensional turbulence persists for a very long time as evidenced by Lielausis (1975). The turbulence level and its properties must be such that they allow a global balance between the energy input due to the instability of the mean flow and the Hartmann dissipation.

The experimental evidence of an inverse energy cascade in a quasi-two-dimensional and almost homogeneous turbulence was given by Sommeria (1986). The only shear in the flow was located along the wall parallel to the magnetic field within a thin layer, where accurate measurements were difficult to realize. So far, the only experiments on MHD turbulent shear flows are those performed by Kljukin & Kolesnikov (1989). They provide interesting data concerning the mean velocity distributions and correlations of velocity fluctuations. But, no information is available about the energy spectra and the development of coherent structures fed by the energy transfer towards the large scales. Experimental data should be of great interest in understanding the physics of these quasi-two-dimensional MHD turbulent shear flows and checking the validity of the recent theoretical work (Pothérat, Sommeria & Moreau 2000; Mück *et al.* 2000). This is precisely the purpose of the MATUR (MAgnetohydrodynamic TURbulence) experiment in Grenoble. The first results obtained from MATUR under a moderate magnetic field ($B = 0.17\,\mathrm{T}$) were presented at the 1997 Turbulent Shear Flow Conference and recently published in Alboussière, Uspenski & Moreau (1999).

The main objectives of the present paper are firstly to provide unique experimental data on MHD turbulent shear flows in a wide range of Ha (B from 0.5 to 6 T) and Re

(current intensity I from 10 to 70 A) numbers, which are of crucial importance for the validation of either numerical or theoretical predictions and, secondly, to highlight the important role of the Hartmann layer which dissipates the kinetic energy by the Joule effect and viscosity. It is shown that, when it dominates the dissipation within the other boundary layers (along walls parallel to the magnetic field), at each wavenumber within the inertial range, this Hartmann dissipation balances the inertial inverse flux of energy. This results in a k^{-3} energy spectra.

A short description of the apparatus and the flow conditions in the MATUR cell is given in § 2. Particular attention is given to the modifications dealing with the high magnetic field (other information can be found in Alboussière *et al.* 1999). Some comments on the diagnostic technique and the data acquisition system are also presented.

Section 3 presents an analysis of the relevant time scales, highlighting those of specific interest for a high magnetic field. The main properties of the mean flow in the unsteady as well as in the quasi-steady regimes are described and discussed in § 4, and the properties of the turbulent velocity fluctuations in the quasi-steady regime are analysed in § 5, followed by some concluding remarks.

2. The experimental set-up

2.1. *General description*

The MATUR cell is a section of a circular cylinder of vertical axis with an internal radius of $R = 11$ cm and a depth of $h = 1$ cm, filled with mercury (see Fig. 1). The bottom plate is electrically insulating, except where small electrodes are inserted. The upper surface is an electrically insulating cover with a mechanism for filling the cell with mercury after a careful cleaning of the cell. The cylindrical wall is made of copper and maintained at a constant and well-controlled temperature by a water cooling system. The internal surface of the wall is protected from the mercury by an electrochemical deposit of nickel. A final gold coating on this surface, which is used as a cathode, ensures a good electric contact with the mercury.

Very small electrodes (1 mm diameter and 1.42 mm apart) are inserted into the bottom plate through holes machined along two concentric circles located 5.4 cm (medium electrodes) and 9.3 cm (external electrodes) away from the cell centre. One of the two circles is used as the anode. A precisely controlled DC current is supplied by a current generator and passes through the mercury from the anode to the wall. Special care is taken that the parallel circuits between the generator and each electrode have exactly the same electric resistance, leading to a uniformly distributed electric current along the electrode ring. The use of a large number of small electrodes instead of a continuous electrode ring is essential to avoid an electrically conducting circuit at a given electric potential (the continuous electrode ring would induce a strong local damping, whereas this effect is minimized on the scale of each individual electrode). Provided the Hartmann number is large enough ($Ha \gg 1$, this is always the case), the electric current intensity I divides in two equal parts (this partition takes place within the free shear layer located just above the electrodes) crossing the two symmetric Hartmann layers. Therefore, the fluid annular domain located between the selected circular electrodes and the cathode ($R_i < r < R$) is driven in rotation by the Lorentz force, while the central fluid domain ($0 < r < R_i$) is entrained by friction within the free shear layer. It is one of the well-established properties of the Hartmann layer that the core mean velocity U_θ is proportional to the current per unit length within

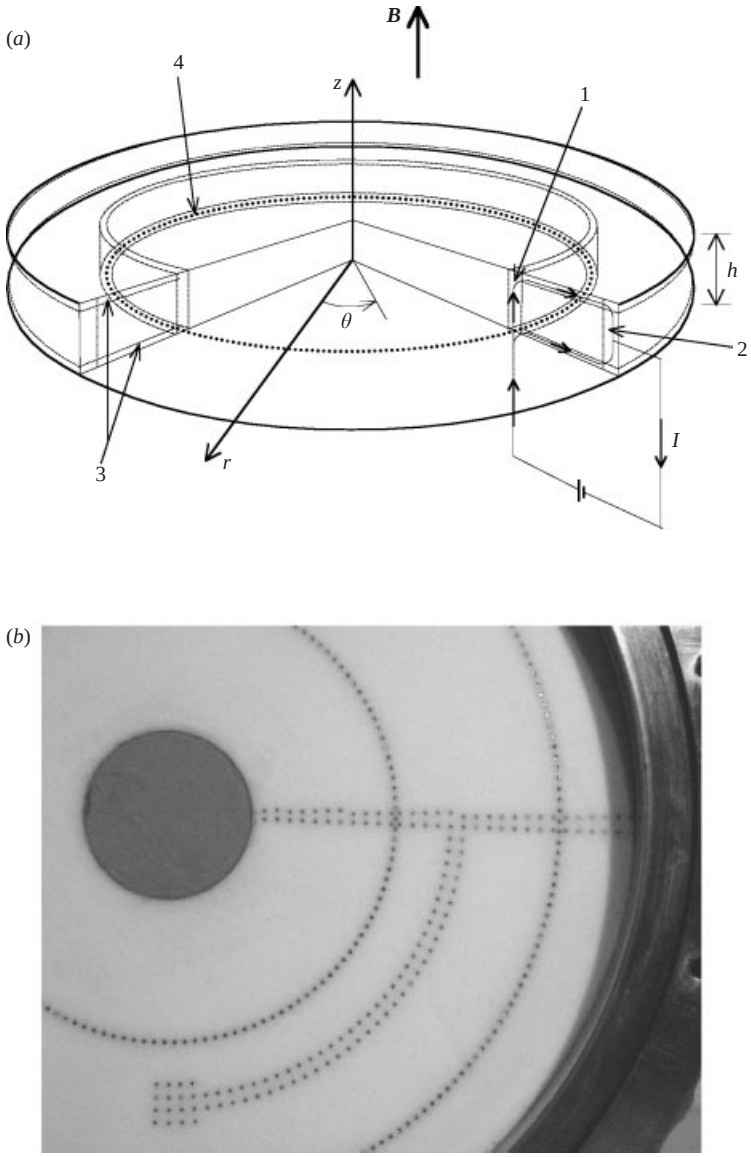

FIGURE 1. (*a*) Sketch of the experimental set up: 1. free shear layer; 2. wall shear layer; 3. Hartmann layers; 4. ring of electrodes. (*b*) Upper view of the bottom plate showing the two electrode rings and the potential probes.

the Hartmann layer ($I/4\pi r$), so that

$$U_\theta = \frac{I}{4\pi r\sqrt{\sigma\rho\nu}}. \tag{2.1}$$

Therefore, the electric current I appears as the main control parameter, while the magnetic field B mainly acts in establishing the two-dimensionality within the core and controlling the dissipation within the Hartmann layers. Between the moving fluid annulus and the internal fluid domain, the shear layer should have a thickness varying as $h\,Ha^{-1/2}$ according to the laminar theory (Hunt & Ludford 1967). But, in this range

of parameters ($I \geqslant$ a few amps), instabilities develop across this layer where the Joule damping is quite limited because of the quasi-two-dimensionality. These instabilities are the source of the turbulence. In fact, the MATUR experiment could be used to observe and characterize this instability, but this is not the purpose of this paper. It is clear from our measurements, however, that instability starts at quite small values of the electric current ($I \lesssim 1$ A) and that above 10 A a well-established turbulent regime sets in.

The central part of the bottom plate is made of thick copper (4 cm diameter), electrically insulated from the mercury, and may be uniformly heated at a given power. This allows an investigation of the turbulent transport of a scalar quantity, such as the temperature, from the central part of the cell towards the external wall which is maintained at a constant temperature.

2.2. *Measurement techniques*

The velocity measurements are performed with a large number of electric potential probes (up to 140 as shown in Fig. 1) inserted into the bottom plate. In fact, it is well known that, when $Ha \gg 1$, the electric potential only has a negligible variation both through the quasi-two-dimensional core and the Hartmann layers. Therefore, the probes located in the plane of the Hartmann wall record the same electric potential as if they were in the turbulent core flow. The electrodes and probes have a non-negligible influence, because they yield a non-zero electric conductance to the wall and contribute to some extra damping of the flow. This effect which is quite small, because the Hartmann number based on the electrodes/probes diameter is small, is acceptable. In fact, there is a tendency to form some MHD columns similar to the Taylor columns on the scale of each electrode, but their diameters are so small that these columns cannot extend from one Hartmann wall to the other. While they stay imbedded within the Hartmann layer, their influence remains negligible.

The key idea of the measuring technique is the property of MHD quasi-two-dimensional core flows according to which Ohm's law is reduced to $\boldsymbol{E} + \boldsymbol{u} \times \boldsymbol{B} = \boldsymbol{0}$ at the first order of Ha^{-1}. Also, across the Hartmann layer the electric potential has a negligible variation of the order of Ha^{-2} (Moreau 1990). Then, the two components of the core velocity $\boldsymbol{u}$ can be derived from the two components of the local electric field using the relation

$$u_r, u_\theta = \frac{1}{B}\left(-\frac{1}{r}\frac{\partial \varphi}{\partial \theta}, \frac{\partial \varphi}{\partial r}\right), \tag{2.2}$$

where u_θ and u_r are the angular and radial components respectively, θ and r denote the angular and radial coordinates, φ is the electric potential. This technique is quite accurate especially for high magnetic field intensity B, where the signal to noise ratio is above 100. The output signal is systematically amplified thanks to a very low-noise amplification system available in our laboratory (see Davoust *et al.* 1999). It must be noted that this diagnostics has no inertia since the electric potential at the wall instantaneously follows the fluid velocity and does not require any calibration.

We also compared these velocity measurements with results from an ultrasonic Doppler velocity measurement technique, which allowed us to check the quasi-two-dimensionality of the flow and confirmed the validity of our measurement procedure.

	$B = 0.5\,\mathrm{T}$ $(Ha = 150)$	$B = 5\,\mathrm{T}$ $(Ha = 1500)$
$\tau_J = \dfrac{\rho}{\sigma B^2}$ (s)	10^{-2}	10^{-4}
$\tau_{2D} = \dfrac{\rho}{\sigma B^2}\dfrac{h^2}{l_\perp^2}$ (s)	10^{-1}	10^{-3}
$\tau_{tu} = \dfrac{l_\perp}{U}$ (s)	1	1
$\tau_H = \dfrac{h}{B}\sqrt{\dfrac{\rho}{\sigma\nu}}$ (s)	10	1
$\tau_\nu = \dfrac{l_\perp^2}{\nu}$ (s)	10^3	10^3

TABLE 1. Key time scales

3. Time scales of interest in a high magnetic field

In the present experiment, at least five important phenomena may be distinguished, whose specific time scales are as follows: the development of the anisotropy induced by the Joule damping ($\tau_J = \rho/\sigma B^2$), the establishment of the two-dimensionality ($\tau_{2D} = (\rho/\sigma B^2)(h^2/l_\perp^2)$), the energy transfer between transverse scales ($\tau_{tu} = l_\perp/U$), the Hartmann dissipation within the Hartmann layers ($\tau_H = (h/B)\sqrt{\rho/\sigma\nu}$), and the viscous effects ($\tau_\nu = l_\perp^2/\nu$). Table 1 gives the order of magnitudes of these time scales for two values of B (0.5 and 5 T). The velocity and the length scales are kept constant ($U = 0.1\,\mathrm{m\,s^{-1}}$, $l_\perp = 10\,\mathrm{cm}$ and $h = 1\,\mathrm{cm}$). The merits of the high magnetic fields become clear, since the establishment of two-dimensionality takes place almost instantaneously ($\tau_{2D} \ll \tau_{tu}$) and the viscous effects are negligible ($\tau_{tu} \ll \tau_\nu$). The only relevant phenomena then are the energy transfer between the different scales (time scale τ_{tu}) and the Hartmann dissipation (time scale τ_H). This explains why the properties of the turbulent flow in this regime depend on only one basic non-dimensional parameter, namely

$$\frac{\tau_{tu}}{\tau_H} = \sqrt{\frac{\sigma}{\rho\nu}}Bh\frac{\nu}{ul_\perp}\frac{l_\perp^2}{h^2} = \frac{Ha}{Re}\left(\frac{l_\perp}{h}\right)^2, \tag{3.1}$$

as mentioned in a number of previous papers (Lielausis 1975; Sommeria & Moreau 1982).

This parameter is proportional to Ha/Re, since the current density within the core ($\sim \sigma Bu/Ha$) is Ha times smaller than within the Hartmann layer ($\sim \sigma Bu$). The ratio between the Lorentz force and inertia in the turbulent core therefore is of the order of Ha/Re (and not of the order of $N = Ha^2/Re$, the interaction parameter).

It may be considered that, when the ratio τ_{tu}/τ_H is small, the dissipation is small enough to leave the energy transfer almost unchanged all through the inertial range. Then, the energy spectrum is that of the expected inverse energy cascade exhibiting a $k^{-5/3}$ power law. On the other hand, when the ratio τ_{tu}/τ_H is large, the dissipation is significant on all relevant scales, so that the energy flux through the cascade cannot be constant. As a result, a Kolmogorov cascade is impossible even with an energy transfer towards the large scales. The energy level at any wavenumber k is controlled

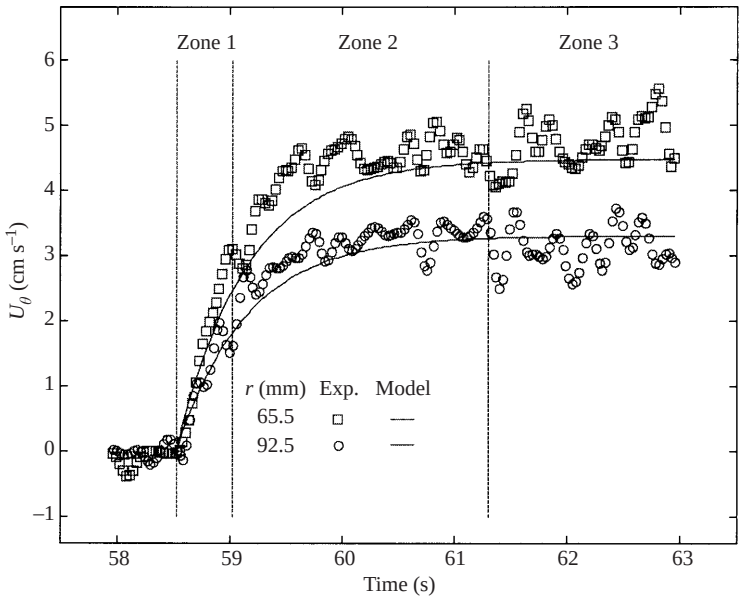

FIGURE 2. Typical angular velocity signals in the unsteady regime measured at two radial positions. I increases from 0 to 3 A at $t \approx 58.6$ s and $B = 4$ T.

by the competition between the local inertial transfer mechanism ($\tau_{tu} \sim 1/\sqrt{k^3 E(k)}$) and the local dissipation in the Hartmann layers ($\tau_H = (h/B)\sqrt{\rho/\sigma\nu}$ which is k-independent). The equality between τ_{tu} and τ_H suggests a k^{-3} energy spectrum at wave numbers smaller than the forcing wavenumber k_i. It must be noted that such a k^{-3} energy spectrum corresponds to an inverse energy cascade modified by the Hartmann damping and not to a direct enstrophy cascade, as will be pointed out in § 5.2. The high magnetic fields are therefore of particular interest, since they provide the possibility of simple dimensional argument in the interpretation of the dominant phenomena.

4. Properties of the mean flow

4.1. *The unsteady regime*

In this section the velocity field during the unsteady phase after a sudden application of the electric current is characterized. Two angular temporal velocity signals measured in the outer region ($r > R_i$) are displayed in Fig. 2. Three different zones may be defined.

The first zone corresponds to the acceleration of the liquid in a laminar regime. The dashed line between zones 1 and 2 corresponds to the transition from the laminar regime to a turbulent regime due to the instability of the shear layer. This kind of shear flow which exhibits an inflectional mean velocity profile is known to be strongly unstable. In zone 2, the acceleration of the fluid shows two important features. The first is the birth of vortices and the second is related to the interactions between them. The third zone corresponds to the ultimate regime of fluid flow with unsteady quasi-two-dimensional vortices. The turbulent signal in this zone is more intermittent than that in zone 2 and could provide information about the large-eddy typical length scale.

The evolution of the mean angular velocity during this unsteady regime may be predicted analytically using a laminar model. Assuming that the electric current and the fluid velocity have one non-zero component j_r and U_θ, the functional dependence of j_r and U_θ in the external fluid annulus can be expressed as

$$j(r,z,t) = j_{Ha}(r,t)\exp(-Haz/h) + j(r,t), \tag{4.1}$$

$$U(r,z,t) = U_\theta(r,t)(1-\exp(-Haz/h)), \tag{4.2}$$

where U_θ is the mean angular velocity of the core flow, z the coordinate parallel to B, and j the electric current in the core flow.

The property of the Hartmann layer yields

$$j_{Ha}(r,t) = -\sigma B U_\theta(r,t). \tag{4.3}$$

The total electric current between the electrodes and the external wall is

$$I = 2\pi r h j(r,t) + 2\pi r h \frac{j_{Ha}(r,t)}{Ha}. \tag{4.4}$$

Now, by neglecting the convective and viscous terms, the Navier–Stokes equation in the core flow is reduced to

$$\rho\frac{\partial U_\theta}{\partial t} = -j_c B. \tag{4.5}$$

We obtain four algebraic equations (4.1)–(4.4) and one differential equation (4.5) for five unknowns with the initial condition $U_\theta = 0$ at $t = 0$. The solution for the core mean velocity in the presence of two symmetric Hartmann layers is

$$U_\theta(r,t) = \frac{I}{4\pi r\sqrt{\sigma\rho\nu}}\left(1-\exp\left(-\frac{\nu Ha}{h^2}t\right)\right). \tag{4.6}$$

The mean velocity $U_\theta(t)$ is plotted in Fig. 2 for two values of r and compared to the experimental results obtained under the same conditions. Good agreement can be seen both at the beginning of zone 1 (initial acceleration) and during the quasi-steady regime (zone 3). The initial agreement is due to the fact that the nonlinear terms of the Navier–Stokes equation are still negligible in this final phase. In particular, this agreement confirms the relevance of the simplified equation (4.5) where j is derived from the Hartmann layer theory. However, a disagreement between the model and the recorded velocity is seen at the beginning of zone 2. In fact, the time needed to reach 90% of the stationary mean velocity is shorter than that predicted by the model (the error bars, as for all the figures presented in this paper, are indicated by the size of the symbols). The nonlinear terms, which are not considered in this model, are responsible for transferring energy between the different scales of turbulence. The resulting mixing of momentum leads to the long term regime being reached in a time τ_1 shorter than τ_2 (see Fig. 2). This could be easily checked in (4.6) if the viscosity ν is replaced by a turbulent viscosity ν_t (where of course $\nu_t > \nu$).

Notice that, as the exponential term of (4.6) vanishes, the core velocity in zone 3 is dictated only by the electric current within the Hartmann layers.

4.2. *The free shear layer*

The radial profiles of the mean angular velocity in the quasi-steady regime are presented in Fig. 3 by way of example. These profiles are obtained using either the medium electrodes ($R_i = 54$ mm, Fig. 3*a*, *c*) or the external ones ($R_i = 93$ mm, Fig. 3*b*, *d*), at different values of I and B.

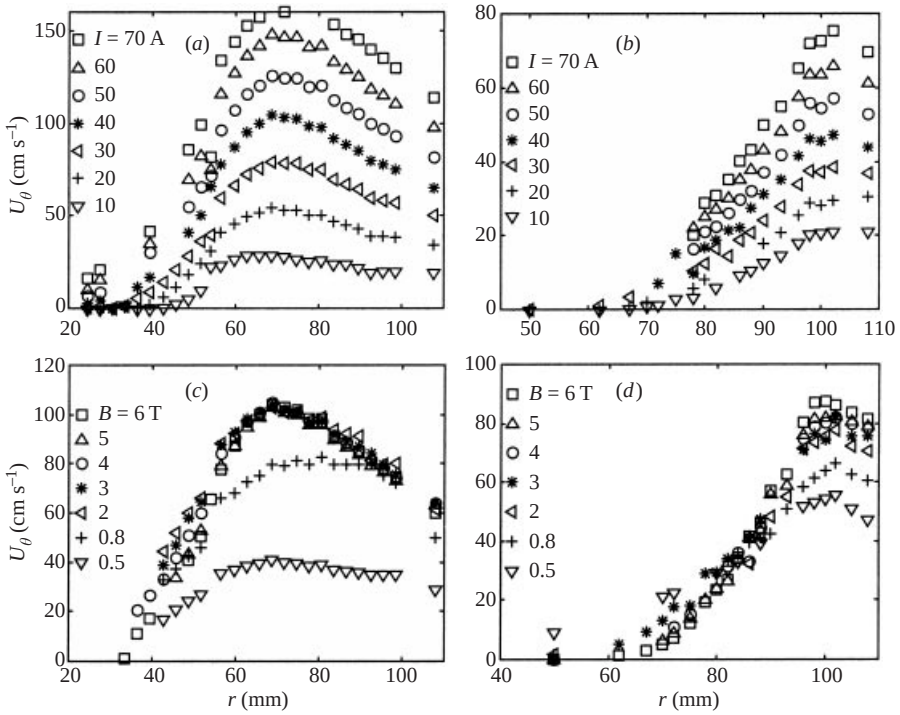

FIGURE 3. Radial profiles of the angular mean velocity. (*a*) $B = 5\,\mathrm{T}$ and $R_i = 54\,\mathrm{mm}$, (*b*) $B = 5\,\mathrm{T}$ and $R_i = 93\,\mathrm{mm}$, (*c*) $I = 40\,\mathrm{A}$ and $R_i = 54\,\mathrm{mm}$, (*d*) $I = 40\,\mathrm{A}$ and $R_i = 93\,\mathrm{mm}$.

The turbulence generated by the instability of the mixing layer transports a fraction of the momentum from the fluid annulus to the inner fluid domain. The resulting entrainment of the fluid in the inner domain is characterized by the decay of the maximum value of U_θ compared to that predicted by the laminar theory.

It is observed that the wall layer remains stable and thin in a wide range of values of the key parameters I and B, independently of the injection radius R_i (Fig. 3). The properties of the shear layer associated with the external set of electrodes could be different from those of a classical free shear layer, since it develops in the vicinity of the wall and may interact with the wall side layer. As a consequence, only data associated with the medium electrodes are presented.

In order to determine the thickness of the shear layer and its dependence on I and B, mean angular velocity profiles (as those plotted in Fig. 4) are used. Let us define the thickness, $\delta_\parallel$, of the shear layer as

$$\delta_\parallel = \frac{\Delta U_\theta}{(\mathrm{d}U/\mathrm{d}r)_{max}}, \tag{4.7}$$

where $\Delta U_\theta = U_{\theta max} - U_{\theta min}$, $U_{\theta min} = 0$, and $U_{\theta max}$ is the mean velocity value at the intersection of the maximum slope (dotted line) and the mean velocity profile (solid line) predicted by the laminar theory (Fig. 4).

It is found that the non-dimensional layer thickness $\delta_\parallel/h$ depends on both Re and Ha according to the relation (Fig. 5)

$$\delta_\parallel/h = C\left(\frac{Ha}{Re}\right)^{-n} \tag{4.8}$$

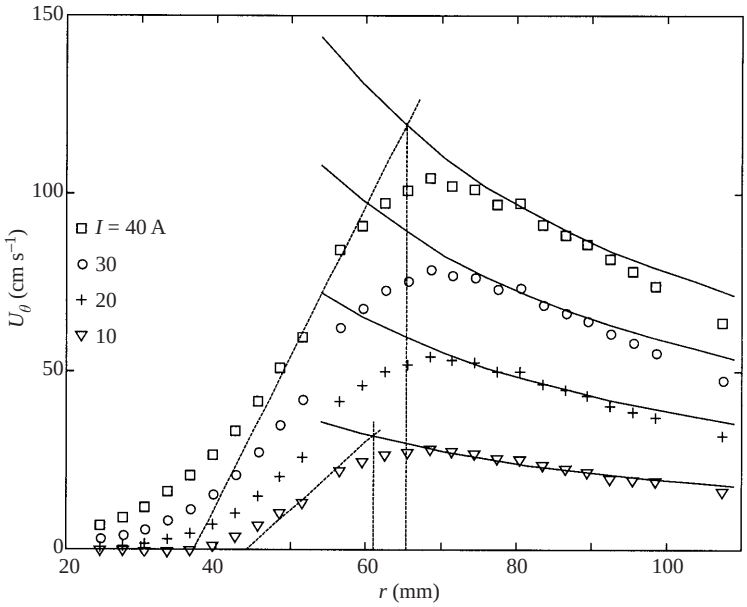

FIGURE 4. Angular mean velocity profiles plotted for $B = 3$ T and for $I = 10$, 20, 30 and 40 A. The solid lines correspond to the angular mean velocity evolution predicted by the laminar theory and the dotted lines to the maximum slopes $(\mathrm{d}U_\theta/\mathrm{d}r)_{max}$ of the experimental profiles.

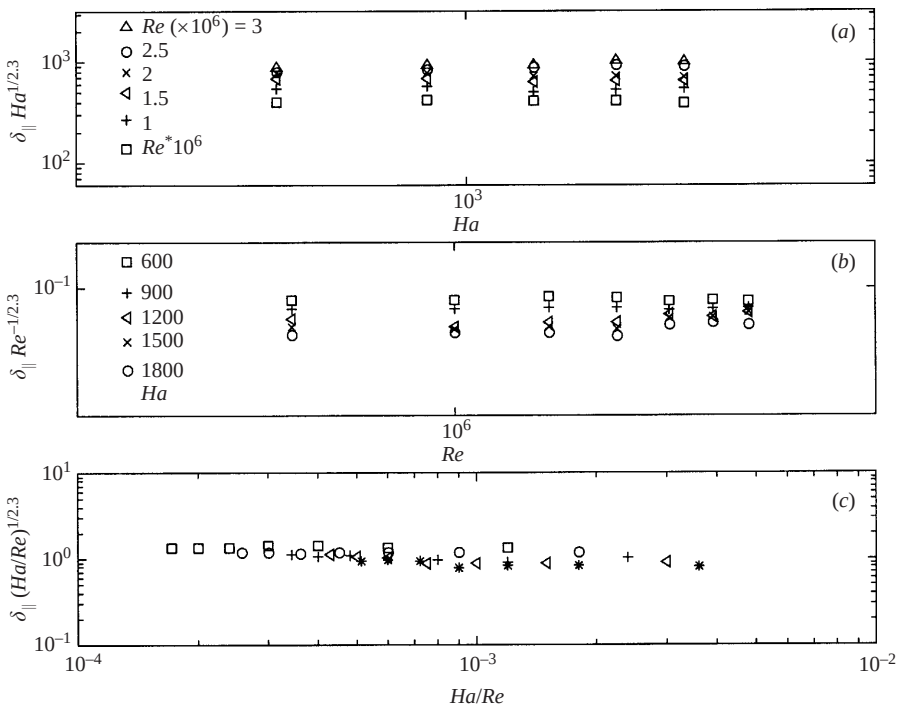

FIGURE 5. Log-log plots of the free turbulent shear layer thickness $\delta_\parallel$. (*a*) Evolution of $\delta_\parallel Ha^{1/2.3}$ with Ha. (*b*) Evolution of $\delta_\parallel Re^{-1/2.3}$ with Re. Both (*a*) and (*b*) suggest that $\delta_\parallel/h \propto (Ha/Re)^{-n}$ with n between $\frac{1}{2.3}$ and $\frac{1}{2.2}$ (see *c*).

with n in the range between $\frac{1}{2.3}$ and $\frac{1}{2.2}$. The best fit suggested by our data for the constant is $C \simeq 1$ (Fig. 5*c*). This dependence, which is quite different from that predicted by the laminar theory ($\delta_{\|L}/h = Ha^{-1/2}$), for which Re has no effect, expresses the effect of turbulence increasing the mixing region as Re increases.

A simple model aiming to explain this experimentally found law (4.8) is proposed. It is based on the quasi-steady equilibrium between the energy transfer and the Hartmann damping in the range of wavenumbers k such that $k_\varrho < k < k_i$ (k_ϱ stands for the integral-length-scale wavenumber and k_i for the injection wavenumber, see Fig. 6). In this model, the energy flux ε_i is assumed to be injected in the neighbourhood of the wavenumber k_i and locally transferred towards the integral-length-scale wavenumber k_ϱ via an inverse energy transfer mechanism (Kraichnan 1967, 1971; Frisch 1995). In the Fourier space, the energy spectrum $E(k,t)$ obeys (see for instance Moreau 1990)

$$\frac{\partial E(k,t)}{\partial t} = -2\nu k^2 E(k,t) - \frac{2}{\tau_H} E(k,t) + T(k,t) + F(k,t), \tag{4.9}$$

where F is the forcing term ($\int_0^\infty F(k)\,\mathrm{d}k = \varepsilon_i$). Neglecting the viscous term when $k \leqslant k_i$, this equation is reduced in a stationary regime to

$$\frac{2}{\tau_H} E(k) = T(k) + F(k). \tag{4.10}$$

Now, integrating (4.10) from 0 to infinity ($\int_0^\infty F(k)\,\mathrm{d}k = \varepsilon_i$ and $\int_0^\infty T(k)\,\mathrm{d}k = 0$) yields

$$\varepsilon_i = \frac{2}{\tau_H} \int_0^\infty E(k)\,\mathrm{d}k. \tag{4.11}$$

But the local quasi-steady equilibrium between the energy transfer and the Hartmann damping in a range of wavenumbers $k_\varrho < k < k_i$ may be expressed by the following relation:

$$\frac{2}{\tau_H} E(k) = T(k), \tag{4.12}$$

where the transfer function term $T(k)$ may be expressed as

$$T(k) \simeq E\frac{u}{l} \simeq Ek(kE)^{1/2}. \tag{4.13}$$

Coupling (4.12) and (4.13) then yields the following expression for the energy spectrum:

$$E(k) = C\tau_H^{-2} k^{-3}. \tag{4.14}$$

This relation is valid only for $k_\varrho < k < k_i$, where the energy transfer between the wavenumbers k may be assumed to be local. The constant C of (4.14) depends on both ε_i and k_i and may be derived from the following dimensional argument. The local energy flux $\varepsilon(k)$ which is not constant because of the Hartmann damping, may be written dimensionally as

$$\varepsilon(k) = C_1 \tau_H^{-3} k^{-2}, \tag{4.15}$$

and the energy density as

$$E(k) = C_K \varepsilon(k)^{2/3} k^{-5/3}. \tag{4.16}$$

It follows that $C = C_K C_1^{2/3} = C_K \varepsilon_i^{2/3} \tau_H^2 k_i^{4/3}$, where C_K is the Kolmogorov constant.

Now, assuming that ε_H corresponds to a non-negligible fraction of ε_i, we may write

$$\varepsilon_i \simeq \varepsilon_H = \frac{2}{\tau_H} \int_{k_\varrho}^{k_i} E(k)\,\mathrm{d}k. \tag{4.17}$$

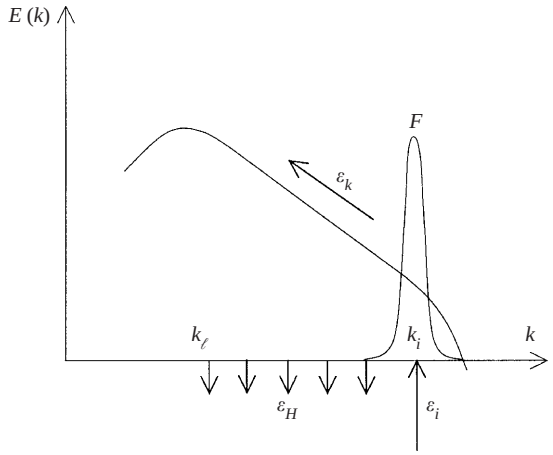

FIGURE 6. Schematic of an inverse energy transfer with a significant energy dissipation by Hartmann braking. The energy flux $\varepsilon_i = \int_0^\infty F(k)\,\mathrm{d}k$ is injected in the neighbourhood of the wavenumber k_i and a fraction of this flux, ε_k, is transferred towards the large scales of the flow.

Assuming also that $k_i^2 \gg k_\varrho^2$,

$$k_\varrho \simeq (C_K\, k_i^{4/3} \varepsilon_i^{-1/3} \tau_H^{-1})^{1/2} \simeq C_K^{1/2} (Lk_i)^{2/3} \frac{1}{h} \left(\frac{Ha}{Re}\right)^{1/2} \tag{4.18}$$

is obtained, where τ_H^{-1} is replaced by $\nu Ha/h^2$ and

$$\varepsilon_i \sim \frac{1}{\tau_{tu}} \langle \boldsymbol{u}^2 \rangle \simeq \frac{U^3}{L} = \frac{(\nu Re)^3}{L^4}.$$

This simple model which expresses the equilibrium between the inertial effect and the Hartmann damping shows that the integral length scale of the flow varies as $(Ha/Re)^{-1/2}$. This prediction gives a first explanation of the observed law of the evolution of the turbulent free shear layer thickness $\delta_\parallel \sim (Ha/Re)^{-1/2.3}$.

4.3. *The global angular momentum*

Another important quantity which may be used to test the theoretical models is the global angular momentum

$$L = \int_{r_{min}}^{r_{max}} r^2 U_\theta(r)\,\mathrm{d}r, \tag{4.19}$$

which is quite significant, since it represents the net effect of the driving torque. In the elementary case of a steady inertialess flow, the Sommeria–Moreau (1982) model yields the simple expression

$$L = \frac{I}{4\pi\sqrt{\rho\sigma\nu}} (r_{max}^2 - r_{min}^2). \tag{4.20}$$

It is the direct consequence of the balance between the driving torque and the opposing (Ohmic and viscous) Hartmann torque (r_{min} and r_{max} are the boundaries of the area where data are available). Note that from this simple balance, the angular momentum can vary linearly with I and be independent of B.

Figure 7 shows the evolution of L with I for different values of B. The solid line corresponds to the theoretical expression (4.20). For $B \geqslant 2$ T ($Ha \geqslant 900$), the

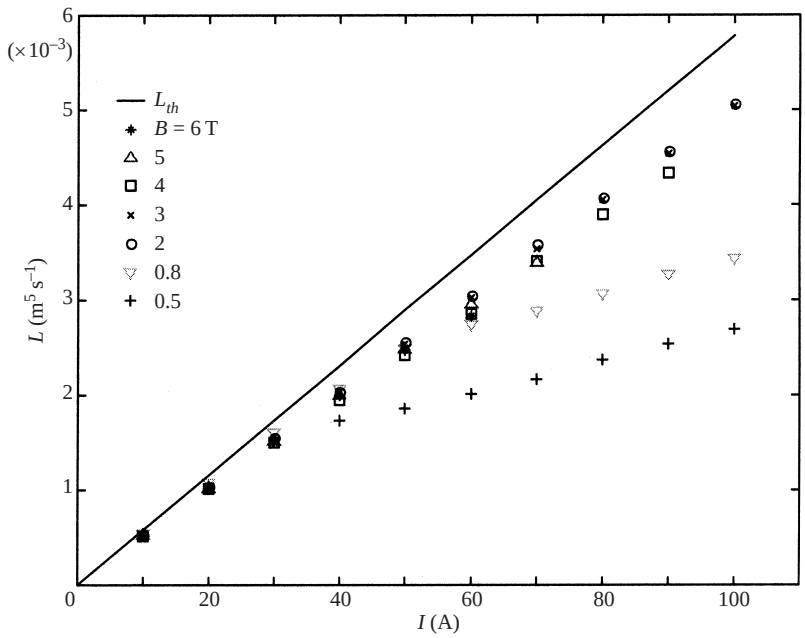

FIGURE 7. Evolution of the angular momentum L versus I for several values of B. The solid line represents the angular momentum evolution predicted by the laminar theory. Note that the linear dependence of L on I, independently of B, at high magnetic fields ($B \geqslant 2$) is a good confirmation of the two-dimensional character of the flow.

variations of L agree with a linear expression similar to (4.20), but have a slope slightly smaller (by 15%) than that predicted by (4.20). This deviation, which cannot be explained by measurement uncertainties, is associated with the extra dissipation originating from the electrically conducting fraction of the bottom wall. Indeed, the global conductivity ratio of this fraction, $C_w = (\sigma_w t_w/\sigma h)S_{cw}/S$ (where S_{cw} is the area of the conducting fraction), yields a correction factor whose order of magnitude ($\simeq 10\%$) may well explain of the deviation between the experimental and theoretical slopes. It should be stressed that the linear dependence of L on I independently of B is a good confirmation of the two-dimensional character of the flow.

Now, for $B < 2$ T, the evolution of L with I exhibits a strong dependence on B. This deviation from the laminar prediction may be interpreted as an effect of Ekman pumping within the Hartmann layers, which enforces a secondary three-dimensional flow that is quite sensitive to the Joule dissipation. This centrifugal secondary flow was modelled recently (Pothérat *et al.* 2000) and a fairly good agreement with our experimental results is found. According to this model, the deviation from the B-independent regime decreases as Ha^2 when Ha increases.

5. Properties of the quasi-two-dimensional turbulence

5.1. *Spectral analysis*

A spectral analysis of the angular velocity fluctuations was performed using Welch's averaged periodogram method. The spatial power spectral densities (PSD) are derived from the temporal velocity signals $u_\theta(t)$ using Taylor's hypothesis. The spatial velocity signals, $u_\theta(x)$, are obtained from $u_\theta(t)$ using the instantaneous velocity instead of the mean velocity, such that $x = u_\theta(t)t$. The PSD estimated in the ranges of $0.5 < B < 6$ T,

$10 < I < 60\,\mathrm{A}$, and $2.3 < r < 10.9\,\mathrm{cm}$ exhibit two important features: first, the presence of peaks at low frequencies (of the order of 1 Hz) and secondly the existence of a short range (less than one decade of k) over which a k^{-n} power law seems to be well defined (Fig. 8). This range is short because it is squeezed between the peaks associated with the large wave scales ($k_\ell \lesssim 0.1\,\mathrm{cm}^{-1}$) and the wavenumber k_i which characterizes the forcing mechanism on small scales ($k_i \simeq 1\,\mathrm{cm}^{-1}$).

It is quite clear that the energy is transferred towards the large scales in this quasi-two-dimensional flow. Figure 8(b) illustrates two examples of compensated energy spectra as $k^3E(k)$, where ranges close to k^{-3} and close to $k^{-5/3}$ can be distinguished. The peaks observed at small wavenumbers (low frequencies) are the signatures of large coherent structures (Fig. 8a).

The shape of the energy spectrum in the intermediate wavenumber range ($k_\ell < k < k_i$) is determined by both the energy transfer mechanism between neighbouring k and the local damping mechanism acting within the Hartmann layers. The spectra exhibit a range close to $k^{-5/3}$ for low values of B and I (typically for $B \leqslant 0.5\,\mathrm{T}$ and $I \leqslant 20\,\mathrm{A}$). Under such conditions, Hartmann damping is small enough to force the energy flux ε towards the large scales to be almost constant (Kraichnan 1967, 1971; Frisch 1995; Lesieur 1997). For larger values of B and I, a range close to k^{-3} is observed within the shear layer, where the turbulence is fully developed. Under these conditions, the dissipation in the Hartmann layers is so significant on all relevant scales that ε cannot be constant. We, thus, believe that the leading effect is the competition between the nonlinear transfer associated with a local transfer time $\tau_{tu} \sim 1/\sqrt{k^3E(k)}$ and the Hartmann damping associated with the k-independent time τ_H. Indeed, the equality of τ_{tu} and τ_H yields such a k^{-3} law and more precisely, suggests the relation

$$E(k) = C\frac{\sigma B^2}{\rho}\frac{v}{h^2k^3} = CHa^2\frac{v^2}{h^4k^3}, \tag{5.1}$$

where the constant C should be universal. Our numerous data suggest a value close to 1.25×10^{-2}.

A remark on the finite size of the probes should be added. The distance d between two neighbouring platinum wires should be taken into account in the PSD calculations. Indeed, the measured velocity fluctuations are the product of the true velocity fluctuations multiplied by a correction factor $C_f = \sin(kd/2)/kd/2$ (see, for instance, Citriniti & George 1997). This correction is only significant in the noise wavenumber range ($k \gtrsim 0.8\,\mathrm{cm}^{-1}$).

5.2. *Energy transfer within the Fourier space*

Many experiments and numerical simulations have been performed to study the inverse cascade of energy in two-dimensional turbulent flows (see, for instance, Sommeria 1986 and Paret & Tabeling 1997 for experiments and Zikanov & Thess 1998 and Crocco & Orlandi 1985 for numerical simulations).

Equation (4.12) shows that the kinetic energy of the core flow is controlled by the term $T(k)$. This term corresponds to the global energy transfer to any wavenumber k by its neighbours. It results from the nonlinear interactions of the Navier–Stokes equation.

For two-dimensional isotropic turbulence, $T(k)$ could be evaluated using triple-velocity correlations at two points as (see, for instance, Nguyen Duc 1988)

$$T(k,t) = \frac{k^2}{4}\int_0^\infty K(r)\, r\, [krJ_0(kr) - 2J_1(kr)]\, \mathrm{d}r, \tag{5.2}$$

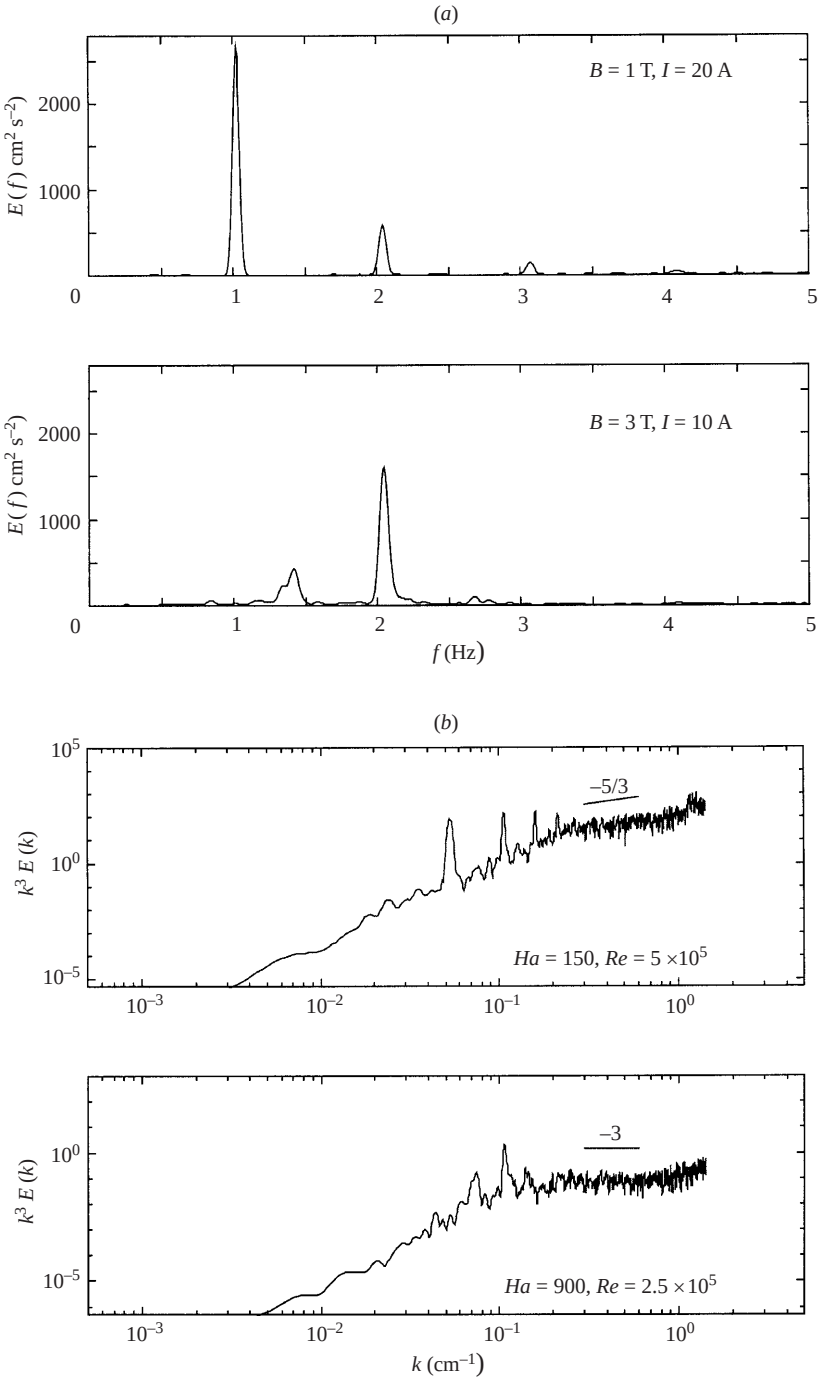

FIGURE 8. (*a*) Frequency spectra of the velocity fluctuations measured within the free shear layer $r \simeq 68.5$ mm. The low frequency peaks are the signature of the large coherent structures. (*b*) Two typical compensated spatial velocity spectra $k^3E(k)$ exhibiting in the inertial range a power law close to $k^{-5/3}$ for $Ha/Re = 6 \times 10^{-4}$ ($B = 1$ T and $I = 20$ A, weak Joule dissipation) and a power law close to k^{-3} for $Ha/Re = 36 \times 10^{-4}$ ($B = 3$ T and $I = 10$ A, important Joule dissipation).

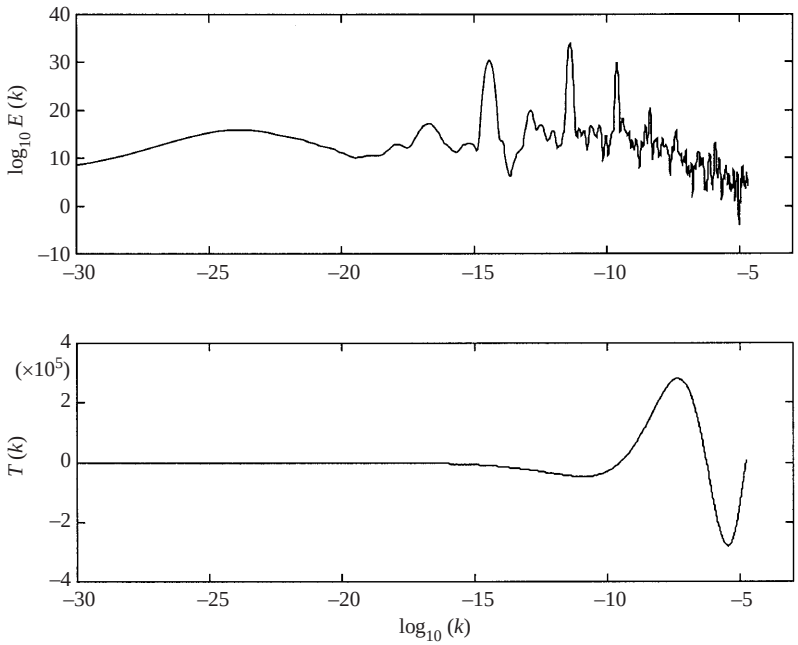

FIGURE 9. Evolution of the energy transfer term $T(k)$ and its associated spatial spectrum $E(k)$. This example illustrates the presence of an inverse energy transfer from large to small wavenumbers in the inertial range. The energy is withdrawn where $T(k) < 0$ and supplied to modes k where $T(k) > 0$.

where

$$K(r) = \langle u(x,0,t)\, u(x,0,t)\, u(x+r,0,t)\rangle \tag{5.3}$$

is a velocity triple-correlation function at two points separated by a distance r, and where J_0 and J_1 are Bessel functions.

Figure 9 shows a typical transfer function $T(k)$ and the corresponding wavenumber spectrum for $B = 0.5\,\mathrm{T}$ and $I = 10\,\mathrm{A}$. This example illustrates the presence of an inverse energy transfer (as previously obtained by Sommeria 1986 and Nguyen Duc & Sommeria 1988) from large to small wavenumbers in the inertial range. The energy is withdrawn where $T(k) < 0$ (close to k_i, corresponding to the instability of the free shear layer) and supplied to modes k where $T(k) > 0$. The negative part of $T(k)$ at low wavenumbers ($1/l \geqslant 0.1\,\mathrm{cm}^{-1}$, outside the inertial range) might be considered as a direct redistribution of the energy from the large to the smallest scales. However, the vorticity maps which have been constructed (see example Fig. 14) clearly show that the maximum size of the large eddies does not exceed half of the box radius. This seems to exclude the presence of a condensation phenomenon (Paret & Tabeling 1997) and, hence, a direct energy cascade on large scales. The fact that the maximum distance r_1 over which the triple-velocity correlations were performed is less than 9 cm suggests that the negative part of $T(k)$ observed at low wave numbers has no real significance and could be the consequence of the non-local energy transfer between different modes.

5.3. *Properties of the large-scale structures*

The properties of the large-scale structures in such flows is of primary interest. In fact, all the transfer phenomena take place in the regions where the shear develops and

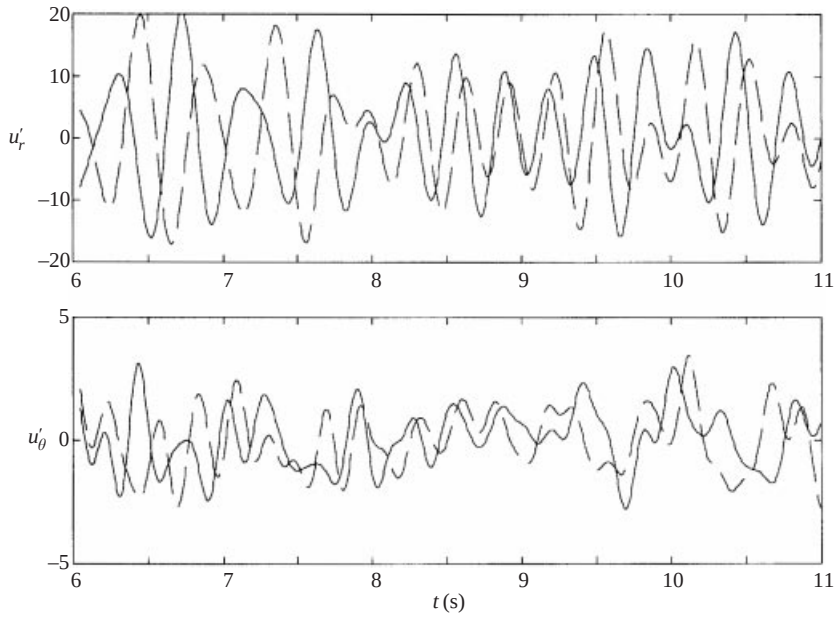

FIGURE 10. Radial and angular velocity filtered signals recorded simultaneously at two different positions ($\theta = 0$ and 0.654 rad). $B = 3\,\mathrm{T}$, $I = 20\,\mathrm{A}$.

the large-scale eddies fed by an inverse energy transfer dominate the flow dynamics. Alboussière *et al.* (1999) demonstrated experimentally (via direct visualizations of the free-surface deformations) that the initial instability of the mixing layer is made up of about 30 periodic eddies (typical length scale $\sim 2\,\mathrm{cm}$) which merge rapidly to form a smaller number of large eddies (2 or 3 with a length scale of $\sim 10\,\mathrm{cm}$). In this section, the influence of the two main parameters, I and B, both on the evolution of the eddy convective velocity and on their average number over one turnover time is studied.

A set of 30 equally spaced probes is inserted into the bottom plate, along an arc of a circle of radius $R_1 = 6.85\,\mathrm{cm}$ (Fig. 1*b*) in order to measure the space–time correlations of the velocity signals. We expect that the trajectory of the large-vortex centres is close to this set of probes. In fact, the velocity signals displayed in Fig. 10 (which are numerically filtered to focus on the large scales only) clearly show that the amplitude of the angular component is much smaller than the radial one. Moreover, it is noticeable that the spatial correlations obtained with the radial velocity component are more significant than those with the azimuthal velocity component.

The transit time $m_j\Delta t$ needed by a large structure to travel from the angular position θ_1 to θ_j corresponds to the integer m_j which maximizes the integral (as illustrated in Fig. 11)

$$\mathrm{Int}(m_j) = \int_{t_0}^{t_1} u_r(\theta_1, t) \cdot u_r(\theta_j, t + m_j\Delta t)\,\mathrm{d}t \tag{5.4}$$

where the radial temporal velocity signals $u_r(\theta_1,\, t = t_0 \rightarrow t_1)$ and $u_r(\theta_j, t = t_0 + m\Delta t \rightarrow t_1 + m\Delta t)$ are recorded simultaneously at the positions θ_1 and θ_j, respectively ($j = \overline{1, 30}$ corresponds to the probe locations) during a time $t_1 + m\Delta t - t_0$ (Δt is a time step fixed by the data sampling frequency).

A maximum of 30 integrals $\mathrm{Int}(m_j)$ could be computed, and for each of them, a

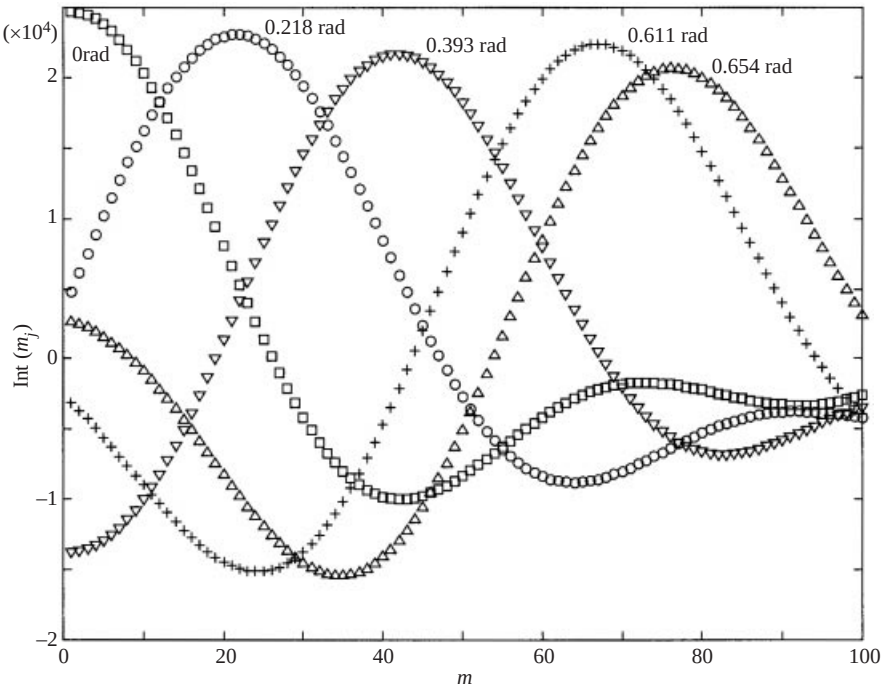

FIGURE 11. Radial velocity cross-correlation functions, Int(m_j). Note that the cross-correlation is about 90% of the auto-correlation for $\theta = \pi/5$, suggesting that the lifetime of the large eddies corresponds at least to their transit time over one turnover time.

transit angular velocity Ω_j is determined by the relation

$$\Omega_j = \frac{\theta_j - \theta_1}{m_j \Delta t}. \tag{5.5}$$

By averaging these angular velocities Ω_j, an estimation of the angular transit velocity $\Omega_S = (1/j)\sum_1^j \Omega_j$ of the large-scale structures is obtained.

The evolution of Ω_S with B and I is shown in Fig. 12. The influence of B remains almost negligible, except for small values of B and large values of I. This is quite consistent with the general idea of the role of the magnetic field being essentially to act to establish two-dimensionality. On the contrary, a strong influence of the electric current I is observed, so that Ω_S is proportional to I and thus to the flow mean velocity U_θ. Figure 11 also shows that for $\theta_j - \theta_1 \lesssim 0.65$ rad ($\simeq \pi/5$) the cross-correlation functions are about 90% of the auto-correlations independently of I and B. This suggests that the large-eddy lifetime at least corresponds to their transit time over one turnover time.

Figure 13 shows an example of linear frequency velocity spectra estimated at different radial locations ($42.5 \leqslant r \leqslant 89.5$ mm) for $B = 5$ T and $I = 20$ A. The spectra are normalized to the maximum value of the PSD in the same distribution. Assuming the coherent structures to be frozen in the flow, it is possible to construct a scenario which gives an estimation of the number of large eddies.

Let us focus on the peaks, whose amplitude is close to unity. Note that the frequency of these peaks is approximately 2 Hz, except in the range of $56.5 \lesssim r \lesssim 62.5$ mm, where it is close to 4 Hz. We may assume that the probes located in this area capture

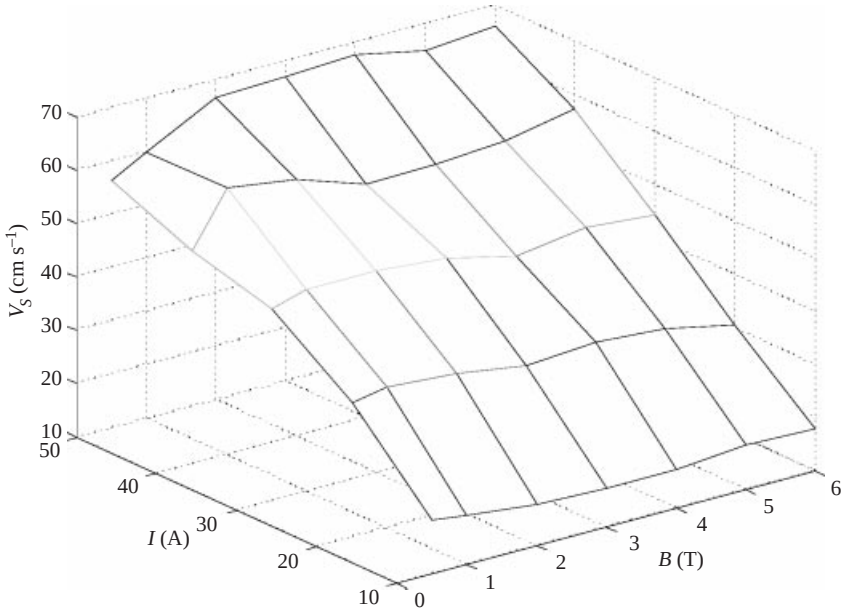

FIGURE 12. Evolution of the transit velocity of the coherent structures $V_S = \Omega_S \times R_1$ with B and I.

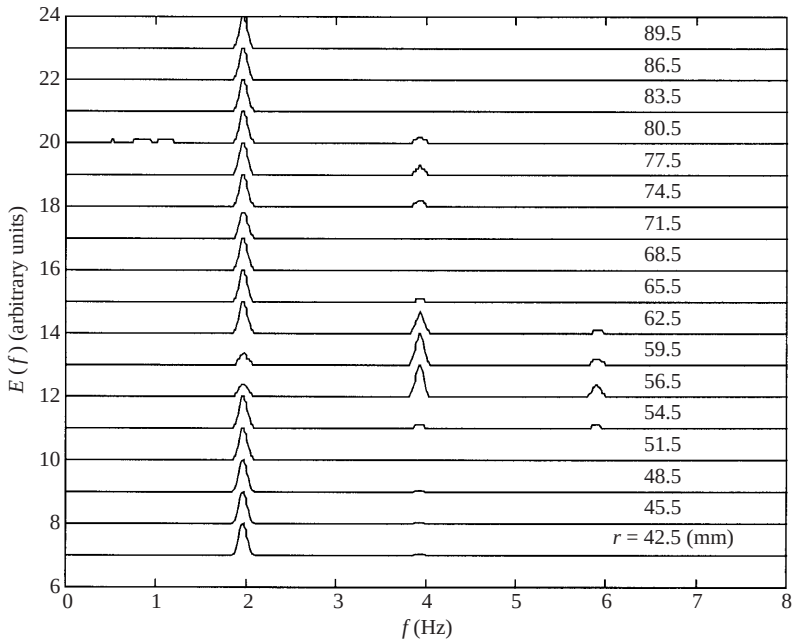

FIGURE 13. Linear frequency velocity spectra at different radial locations suggesting the presence of two pairs of large eddies. $B = 5\,\mathrm{T}$ and $I = 20\,\mathrm{A}$.

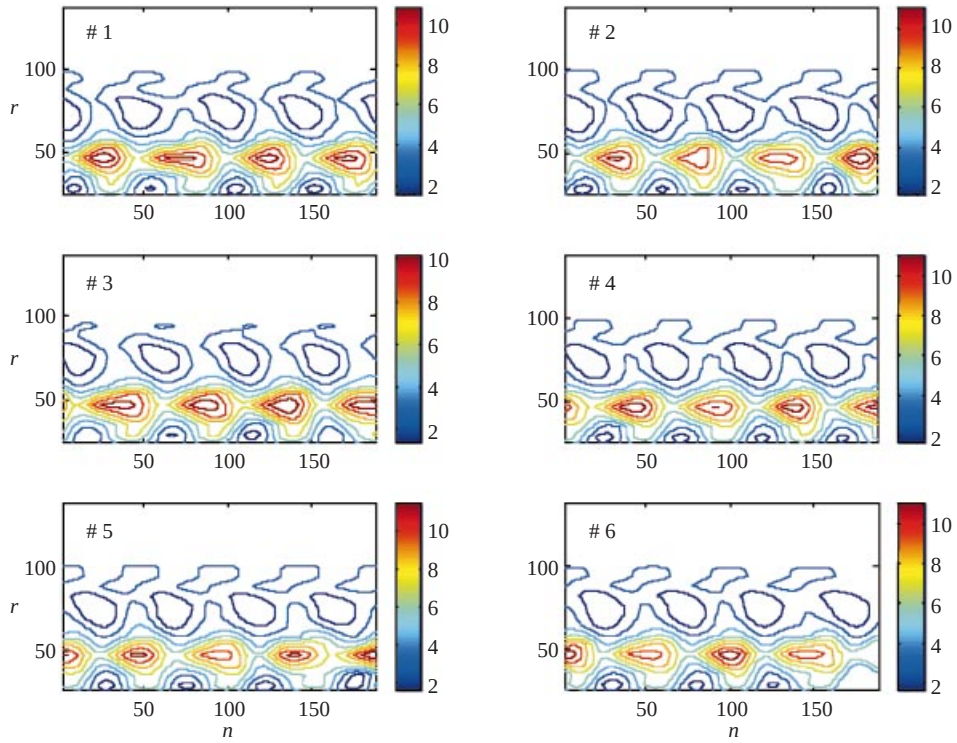

FIGURE 14. Reconstructed vorticity field over 6 turnover times under the same conditions as in figure 12 ($B = 5\,\mathrm{T}$ and $I = 20\,\mathrm{A}$), confirming the presence of four large eddies. For clarity, the vorticity field is plotted on a straight plane.

four structures passing during one turnover time, whereas two eddies are detected by the others. In agreement with this observation, the presence of two pairs of small and large eddies in the basic flow could be assumed. In most cases, the picture is not that simple and an estimation of the number of coherent structures cannot possibly be obtained from a spectral analysis of the turbulent flow. In order to examine the evolution of the number of large structures, we reproduced the whole velocity field in the box by successive rotations of the velocity curves measured on the line probes (angular position θ_0) at times $t_0 + n\Delta t$ (n is the number of rotations). At each time $t_0 + n\Delta t$, the corresponding velocity profile is plotted at the angular position θ_0, whereas the profile recorded at the time t_0 is plotted at the angular position $\Omega_S n\Delta t + \theta_0$. Finally, to make the counting of the large eddies easier, the vorticity field is computed by taking the cylindrical curl of the velocity field and then plotting on a straight plane (Fig. 14).

The vorticity field constructed for the same experimental conditions as those in Fig. 13 confirms that the number of large eddies is 4. Similar computations for different values of B and I allow determination of the variations of the number of these large eddies N_S (Fig. 15a). This points out again the leading role of I, while B has a weak effect on N_S. Comparison of figures 15(a) and 14(b) shows the existence of a reasonable correlation between N_S and the ratio τ_{tu}/τ_H. Figure 15(c) presents the evolution of $N_S \times (Re/Ha)^{0.4}$ versus (Re/Ha) suggesting that $N_S \simeq 80(Ha/Re)^{1/2.5}$. As expected, the number of large coherent structures driven by the flow when the

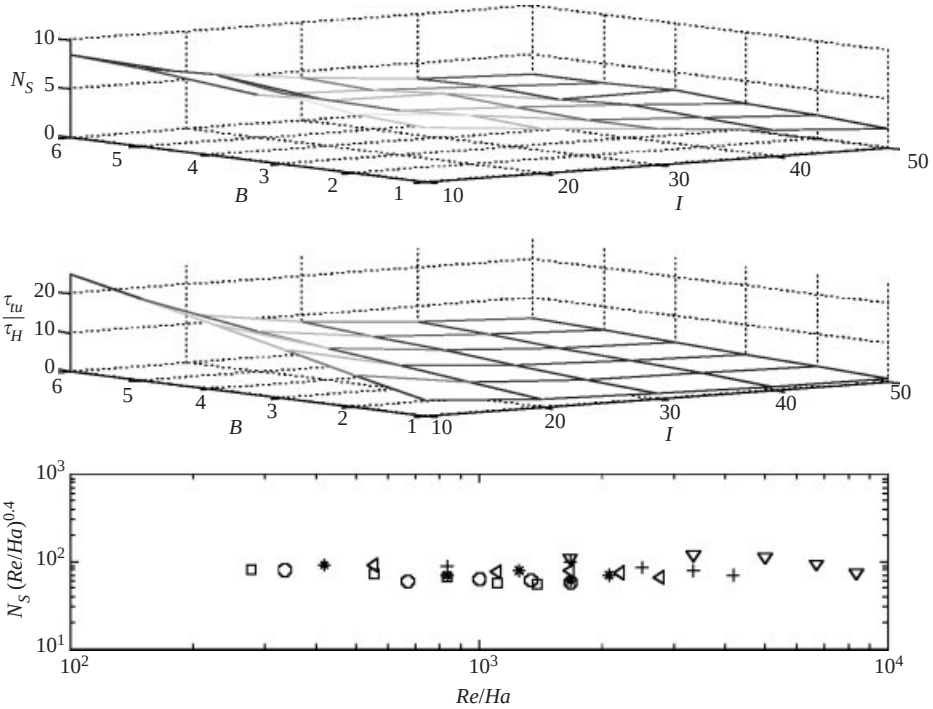

FIGURE 15. (*a*) Evolution of the number of coherent structures N_S with B and I. (*b*) Ratio of the turnover time to the Hartmann damping time τ_{tu}/τ_H versus B and I. (*c*) $N_S \times (Re/Ha)^{0.4}$ versus (Re/Ha) confirms that N_S is dictated by the balance between inertia and the Hartmann damping. $N_S \simeq 80\,(Ha/Re)^{1/2.5}$.

turbulence is fully developed results from a competition between the inertial effects and the damping effect in the Hartmann layers.

6. Concluding remarks

A forced quasi-two-dimensional non-homogeneous turbulence in an electrically conducting fluid subject to a uniform magnetic field is investigated. A detailed quantitative analysis of this statistically steady MHD turbulent shear flow at low R_m is provided. The mixing zone between the moving external annulus and the inner domain is the region of greatest interest, where the turbulence develops and controls the transport of any quantity. It is found that the free shear layer thickness $\delta_\parallel$ is increased by about two order of magnitudes by turbulence, resulting in an enhancement of momentum transport across the layer. Its non-dimensional value $\delta_\parallel/h$ depends on both Ha and Re as $(Ha/Re)^{-1/2.3}$ instead of $Ha^{-1/2}$ as predicted by the laminar theory.

The angular momentum L is found to be in good agreement with the prediction of the two-dimensional model when the magnetic field is large enough to suppress any deviation from two-dimensionality. It is B-independent and varies linearly with the electric current I. The moderate disagreement between the experimental and the theoretical laws $L(I)$ is a result of the effect of the extra dissipation due to the small fraction of the bottom wall which is electrically conducting.

The velocity field is dominated by a small number of large coherent structures fed

by the inverse energy transfer that is characteristic of quasi-two-dimensional forced turbulent flows. Their number seems to be proportional to the ratio Ha/Re and their transit velocity is slightly above $U_{\theta max}/2$. For wavenumbers ranging between the large-structure wavenumber k_ℓ and the forcing wavenumber k_i, an inertial range exhibits a k^{-n} power law where n may be close to either 5/3 or 3. Our interpretation of this inertial law is based on the importance of the Hartmann dissipation (timescale τ_H) in comparison with the eddy turnover time (timescale τ_{tu}). When this dissipation is negligible, a power law close to $k^{-5/3}$ is observed as conjectured by Kraichnan. But when it is significant, the quasi-steady equilibrium at any wavenumber k implies an equality of τ_{tu} and τ_H and leads to the k^{-3} law. This explains the proportionality between C in the law $E = Ck^{-3}$ and the non-dimensional parameter $Ha/Re(l_\perp/h)^2$.

These experiments in a high magnetic field were performed in one of the magnet sources (M5) of the Grenoble High Magnetic Field Laboratory. We are very grateful to V. Uspenski from Moscow University for his effective contribution during the first experiments. Technical assistance by R. Bolcato is gratefully acknowledged. We would also like to thank A. Pothérat, J. Sommeria and T. Alboussière for fruitful discussions. This work was supported first by the European Community under contract No. ERB-CIPA-CT 93-0080 and then by the French Atomic Energy Commission (CEA, centre d'études de Cadarache) under contract No. 5010 6 7B036910.

REFERENCES

Alboussière, T., Neubrand, A. C., Garandet, J. P. & Moreau, R. 1997 Segregation during horizontal Bridgman growth under an axial magnetic field. *J. Cryst. Growth* **181**, 133–144.

Alboussière, T., Uspenski, V. & Moreau, R. 1999 Quasi-two-dimensional turbulent shear layers. *Expl Therm. Fluid Sci.* **20**, 19–24.

Alemany, A., Moreau, R., Sulem, P. & Frish, U. 1979 Influence of an external magnetic field on homogeneous MHD turbulence. *J. Méc.* **18**, 277–313.

Citriniti, J. H. & George, W. K. 1997 The reduction of spatial aliasing by long hot-wire anemometer probes. *Exps. Fluids* **23**, 217–224.

Crocco, L. & Orlandi, P. 1985 A transformation for the energy-transfer term in isotropic turbulence. *J. Fluid Mech.* **16**, 405–424.

Davidson, P. A. 1995 Magnetic damping of jets and vortices. *J. Fluid Mech.* **299**, 153–186.

Davidson, P. A. 1997 The role of angular momentum in the magnetic damping of turbulence. *J. Fluid Mech.* **336**, 123–150.

Davoust, L., Cowley, M. D., Moreau, R. & Bolcato, R. 1999 Buoyancy-driven convection with a uniform magnetic field. *J. Fluid Mech.* **400**, 59–90.

Frisch, U. 1995 *Turbulence, the Legacy of A. N. Kolmogorov*. Cambridge University Press.

Hunt, J. C. R. & Ludford, G. S. S. 1968 Three-dimensional MHD duct flows with strong transverse magnetic fields. Part 1. Obstacles in a constant area channel. *J. Fluid Mech.* **33**, 693–714.

Kljukin, A. A. & Kolesnikov, Yu. B. 1989 MHD instabilities and turbulence in liquid metal shear flows. *Proc. IUTAM Symposium 'Liquid Metal Magnetohydrodynamics* (ed. J. Lielpeteris & R. Moreau), pp. 449–454. Kluwer.

Kolesnikov, Yu. & Tsinober, A. B. 1972 An experimental study of two-dimensional turbulence behind a grid. *Fluid Dynamics* **9**, 621–624.

Kraichnan, R. H. 1967 Inertial ranges in two-dimensional turbulence. *Phys. Fluids* **10**, 1417–1423.

Kraichnan, R. H. 1971 Inertial range transfer in two and three dimensional turbulence. *J. Fluid Mech.* **47**, 525–535.

Lenhert, B. 1955 Instability of laminar flow of mercury caused by an external magnetic field. *Proc. R. Soc. Lond.* A **233**, 299–301.

Lesieur, M. 1997 *Turbulence in Fluids*. Kluwer.

Lielausis, O. A. 1975 Liquid metal magnetohydrodynamics. *Atomic Energy Review* **13**, 527–581.

Moreau, R. 1990 *Magnetohydrodynamics*. Kluwer.

MÜCK, B., GÜNTER, C., MÜLLER, U. & BÜHLER, L. 2000 Three-dimensional MHD flows in rectangular ducts with internal obstacles. *J. Fluid Mech.* **418**, 265–295.

NGUYEN DUC, J. M. 1988 Instabilité et turbulence dans des écoulements bidimensionnels MHD. Thèse de Doctorat de l'Institut National Polytechnique de Grenoble.

NGUYEN DUC, J. M. & SOMMERIA, J. 1988 Experimental characterization of steady two-dimensional vortex couples. *J. Fluid Mech.* **192**, 175–192.

PARET, J. & TABELING, P. 1997 Experimental observation of the two-dimensional inverse energy cascade. *Phys. Rev. Lett.* **79**, 4162–4165.

PARET, J. & TABELING, P. 1998 Intermittency in the two-dimensional inverse cascade of energy: experimental observations. *Phys. Fluids* **10**, 3126–3136.

POTHÉRAT, A., SOMMERIA, J. & MOREAU, R. 2000 An effective two-dimensional model for MHD flows with transverse magnetic field. *J. Fluid Mech.* **424**, 75–100.

SOMMERIA, J. 1986 Experimental study of two-dimensional inverse energy cascade in a square box. *J. Fluid Mech.* **170**, 139–168.

SOMMERIA, J. & MOREAU, R. 1982 Why, how and when MHD turbulence becomes two-dimensional? *J. Fluid Mech.* **118**, 507–518.

ZIKANOV, O. & THESS, A. 1998 Direct numerical simulation of forced MHD turbulence at low magnetic Reynolds number. *J. Fluid Mech.* **358**, 299–333.